Wind and Structures, Vol. 10, No. 5 (2007) 421-435
DOI: http://dx.doi.org/10.12989/was.2007.10.5.421

Investigation on flutter mechanism of long-span bridges with 2d-3DOF method

Yongxin Yang†, Yaojun Ge‡ and Haifan Xiang‡†

State Key Lab for Disaster Reduction in Civil Engineering, Tongji University, Shanghai, China
(Received May 8, 2006, Accepted August 31, 2007)

Abstract. A two-dimensional flutter analysis method (2d-3DOF method) was developed to simultaneously investigate the relationship between oscillation parameters and aerodynamic derivatives of three degrees of freedom, and to clarify the coupling effects of different degrees of freedom in flutter instability. With this method, the flutter mechanism of two typical bridge deck sections, box girder section and two-isolated-girder section, were numerically investigated, and both differences and common ground in these two typical flutter phenomena are summarized. Then the flutter stabilization effect and its mechanism for long-span bridges with box girders by using central-slotting were studied by experimental investigation of aerodynamic stability and theoretical analysis of stabilizing mechanism. Possible explanation of new findings in the evaluation trend of critical wind speed through central vent width is finally presented.

Keywords: aerodynamic instability; flutter analysis; long span bridge; coupling effect; flutter mechanism; central slotting; vent width.

1. Introduction

With the rapid increase of span length, bridge structures are becoming more flexible and more sensitive to wind action. Among all the wind-induced responses of long-span bridges, flutter is the most dangerous phenomenon. After the infamous incident of the original Tacoma Narrows Bridge, there were attempts to explain the wind induced bridge vibration as something similar to what had been known as an airfoil flutter. The difficulty then was the fact that the wind forces acting on an aerodynamically bluff section such as of the bridge deck should be altogether different from the case of a streamlined airplane wing and could not be calculated by any analytical means. This left the issues both for practical design purposes and for theoretical clarification of flutter-driven mechanisms with the scaled model tests in wind tunnels or analysis methods using parameters obtained from wind tunnel tests.

Since then, flutter theory and corresponding calculation methods have got a rapid progress especially in the last two decades. But as for the problem of flutter mechanism, there is still much work needed to be done. Although three-dimensional flutter analysis methods based on finite

† Associate Professor, Corresponding Author, E-mail: yang_y_x@mail.tongji.edu.cn
‡ Professor, E-mail: yaojunge@mail.tongji.edu.cn
‡† Professor

element method (FEM) models have the advantage of the calculation precision of flutter critical speed (Ding 2002, Hua 2007), as far as flutter mechanism is concerned, two-dimensional approaches with typical section models are usually more appropriate and more straight forward (Simiu and Scanlan 1996, Como 2005). Because the focuses of three-dimensional flutter analysis methods are the spatial modes of bridge structures and the mode-coupling effects, but the most important problem in flutter mechanism is the formation of the driving force for oscillation divergence (mostly negative aerodynamic damping) or the relationship between oscillation parameters and the aerodynamic configuration of bridge deck sections (two-dimensional sections) which is just the investigation focus of two-dimensional flutter analysis methods, in which the oscillation parameters of bridge structures such as frequencies, damping ratios, critical wind speeds etc., are analyzed using aerodynamic derivatives identified through section model tests, and some important information about the study of flutter mechanism can be obtained (Matsumoto 1995, Xiang 1999, Matsumoto 2000).

In this paper, based on the concept of full-degree coupling analysis, a two-dimensional three-degrees-of-freedom coupling flutter analysis method (2d-3DOF method) was developed to focus on relationship among vibration frequencies, damping ratios and aerodynamic configuration of bridge decks, and the coupling effect of degrees of freedom in flutter instability (Yang 2002, Yang 2003). With this method, the flutter mechanism of two typical bridge deck sections, box girder section and two-isolated-girder section, were numerically investigated. The flutter stabilization effect and its mechanism for long-span bridges with box girders by using central-slotting were also studied by experimental investigation and theoretical analysis. Some new findings in the evolution trend of critical wind speed through central vent width are finally explained.

2. General formulation

For an oscillation system with only one degree of freedom, for example, torsional degree of freedom, the motion equation is simply described by Yang (2002)

$$\ddot{\alpha} + 2\xi_{\alpha 0}\omega_{\alpha 0}\dot{\alpha} + \omega_{\alpha 0}^2\alpha = \frac{\rho B^4}{I}\omega_\alpha A_2^*\dot{\alpha} + \frac{\rho B^4}{I}\omega_\alpha^2 A_3^*\dot{\alpha} \tag{1}$$

where $\xi_{\alpha 0}$ is structural damping ratio of torsional motion, $\omega_{\alpha 0}$ is structural torsional circular frequency, ρ is air mass density, B is bridge deck width, I is structural generalized mass moment of inertia, A_i^* (i=2, 3) are dimensionless aerodynamic derivatives measured in wind tunnel tests. The items on the right side of the equation represent self-excited pitching moment caused by torsional movement of the bridge deck.

2.1. Coupled torsional oscillation

As a matter of fact, a two-dimensional bridge deck section has three degrees of freedom, and the self-excited forces corresponding to each DOF are coupled. This means that not only the torsional motion but also motions of the other two DOFs of a deck section can produce aerodynamic pitching moment. Therefore the self-excited pitching moment on the right side of the motion equation should consist of three parts corresponding to each DOF, and the torsional motion equation can be rewritten as:

$$\ddot{\alpha} + 2\xi_{\alpha 0}\omega_{\alpha 0}\dot{\alpha} + \omega_{\alpha 0}^2\alpha = M_{se}(\alpha, \alpha) + M_{se}(\alpha, h) + M_{se}(\alpha, p) \tag{2}$$

The first part of aerodynamic pitching moment $M_{se}(\alpha, \alpha)$ is caused by the torsional movement of the bridge deck, which is identical to that in Eq. (1).

$$M_{se}(\alpha, \alpha) = \frac{\rho B^4}{I}\omega_\alpha A_2^* \dot{\alpha} + \frac{\rho B^4}{I}\omega_\alpha^2 A_3^* \dot{\alpha} \tag{3}$$

The other two parts $M_{se}(\alpha, h)$ and $M_{se}(\alpha, p)$ are aerodynamic pitching moments induced by the coupling heaving and coupling swaying motion of the bridge deck respectively which are excited by the torsional movement of the bridge deck as follows

$$\begin{aligned} M_{se}(\alpha, h) = \frac{\rho B^4}{I}\frac{\rho B^2}{m_h}\Omega_{h,\alpha}(&\omega_\alpha A_1^* H_2^* \cos\theta_1 \dot{\alpha} + \omega_\alpha^2 A_1^* H_2^* \sin\theta_1 \alpha - \omega_\alpha A_4^* H_2^* \sin\theta_1 \dot{\alpha} \\ &+ \omega_\alpha^2 A_4^* H_2^* \cos\theta_1 \alpha + \omega_\alpha A_1^* H_3^* \cos\theta_2 \dot{\alpha} + \omega_\alpha^2 A_1^* H_3^* \sin\theta_2 \alpha \\ &- \omega_\alpha A_4^* H_3^* \sin\theta_2 \dot{\alpha} + \omega_\alpha^2 A_4^* H_3^* \cos\theta_2 \alpha) \end{aligned} \tag{4}$$

$$\begin{aligned} M_{se}(\alpha, p) = \frac{\rho B^4}{I}\frac{\rho B^2}{m_p}\Omega_{p,\alpha}(&\omega_\alpha A_5^* P_2^* \cos\theta_3 \dot{\alpha} + \omega_\alpha^2 A_5^* P_2^* \sin\theta_3 \alpha - \omega_\alpha A_6^* P_2^* \sin\theta_3 \dot{\alpha} \\ &+ \omega_\alpha^2 A_6^* P_2^* \cos\theta_3 \alpha + \omega_\alpha A_5^* P_3^* \cos\theta_4 \dot{\alpha} + \omega_\alpha^2 A_5^* P_3^* \sin\theta_4 \alpha \\ &- \omega_\alpha A_6^* P_3^* \sin\theta_4 \dot{\alpha} + \omega_\alpha^2 A_6^* P_3^* \cos\theta_4 \alpha) \end{aligned} \tag{5}$$

where $\Omega_{i,j}$ is dimensionless equivalent frequency between motions of different DOFs and is defined as

$$\Omega_{i,j} = \frac{\omega_j^2}{\sqrt{(\omega_i^2 - \omega_j^2)^2 + 4(\xi_i \omega_i)^2 \omega_j^2}} \quad (i, j = \alpha, h, p) \tag{6}$$

and the phase lags between motions of different DOFs are expressed as

$$\theta_1 = \theta_{h\alpha} + 3\pi/2 \tag{7}$$
$$\theta_2 = \theta_{h\alpha} \tag{8}$$
$$\theta_3 = \theta_{p\alpha} + 3\pi/2 \tag{9}$$
$$\theta_4 = \theta_{p\alpha} \tag{10}$$

$$\theta_{h\alpha} = arctg\frac{2\xi_h \omega_h \omega_\alpha}{\omega_h^2 - \omega_\alpha^2} \quad (90^o < \theta_{h\alpha} < 180^o) \tag{11}$$

$$\theta_{p\alpha} = arctg\frac{2\xi_p \omega_p \omega_\alpha}{\omega_p^2 - \omega_\alpha^2} \quad (90^o < \theta_{p\alpha} < 180^o) \tag{12}$$

2.2. Equations of heaving and swaying motions

Similarly, the other two motion equations of heaving and swaying motions can be established and the heaving motion equation is

$$\ddot{h} + 2\xi_{h0}\omega_{h0}\dot{h} + \omega_{h0}^2 h = L_{se}(h, h) + L_{se}(h, \alpha) + L_{se}(h, p) \tag{13}$$

where the detailed three parts of the self-excited lift force corresponding to each DOF are expressed as

$$L_{se}(h,\ h)\ =\ \frac{\rho B^2}{m_h}\omega_h H_1^*\dot{h}+\frac{\rho B^2}{m_h}\omega_h^2 H_4^* h \tag{14}$$

$$\begin{aligned} L_{se}(h,\ \alpha)\ =\ \frac{\rho B^2}{m_h}\frac{\rho B^4}{I}\Omega_{\alpha,h}\ (&\omega_h H_2^* A_1^*\cos\theta_5\dot{h}+\omega_h^2 H_2^* A_1^*\sin\theta_5 h-\omega_h H_3^* A_1^*\sin\theta_5\dot{h}\\ &+\omega_h^2 H_3^* A_1^*\cos\theta_5 h+\omega_h H_2^* A_4^*\cos\theta_6\dot{h}+\omega_h^2 H_2^* A_4^*\sin\theta_6 h\\ &-\omega_h H_3^* A_4^*\sin\theta_6\dot{h}+\omega_h^2 H_3^* A_4^*\cos\theta_6 h \end{aligned} \tag{15}$$

$$\begin{aligned} L_{se}(h,\ p)\ =\ \frac{\rho B^2}{m_h}\frac{\rho B^2}{m_p}\Omega_{p,h}\ (&\omega_h H_5^* P_1^*\cos\theta_7\dot{h}+\omega_h^2 H_5^* P_1^*\sin\theta_7 h-\omega_h H_6^* P_1^*\sin\theta_7\dot{h}\\ &+\omega_h^2 H_6^* P_1^*\cos\theta_7 h+\omega_h H_5^* P_4^*\cos\theta_8\dot{h}+\omega_h^2 H_5^* P_4^*\sin\theta_8 h\\ &-\omega_h H_6^* P_4^*\sin\theta_8\dot{h}+\omega_h^2 H_6^* P_4^*\cos\theta_8 h \end{aligned} \tag{16}$$

and the phase lags are

$$\theta_5=\theta_{\alpha h}+3\pi/2 \tag{17}$$
$$\theta_6=\theta_{\alpha h} \tag{18}$$
$$\theta_7=\theta_{ph}+3\pi/2 \tag{19}$$
$$\theta_8=\theta_{ph} \tag{20}$$

$$\theta_{\alpha h}\ =\ arctg\frac{2\xi_\alpha\omega_\alpha\omega_h}{\omega_\alpha^2-\omega_h^2}\ (0^o<\theta_{\alpha h}<90^o) \tag{21}$$

$$\theta_{ph}\ =\ arctg\frac{2\xi_p\omega_p\omega_h}{\omega_p^2-\omega_h^2}\ (\omega_p>\omega_F,\ 0^o<\theta_{ph}<90^o;\ \omega_p>\omega_F,\ 90^o<\theta_{ph}<180^o) \tag{22}$$

Finally the swaying motion equation is

$$\ddot{p}+2\xi_{p0}\omega_{p0}\dot{p}+\omega_{p0}^2 p\ =\ D_{se}(p,\ p)+D_{se}(p,\ \alpha)+D_{se}(p,\ h) \tag{23}$$

where the detailed three parts of the self-excited drag force corresponding to each DOF are expressed as

$$D_{se}(p,\ p)\ =\ \frac{\rho B^2}{m_p}\omega_p P_5^*\dot{p}+\frac{\rho B^2}{m_p}\omega_p^2 P_6^* p \tag{24}$$

$$\begin{aligned} D_{se}(p,\ \alpha)\ =\ \frac{\rho B^2}{m_p}\frac{\rho B^4}{I}\Omega_{\alpha,h}\ (&\omega_p P_2^* A_5^*\cos\theta_9\dot{p}+\omega_p^2 P_2^* A_5^*\sin\theta_9 p-\omega_p P_3^* A_5^*\sin\theta_9\dot{p}\\ &+\omega_p^2 P_3^* A_5^*\cos\theta_9 p+\omega_p P_2^* A_6^*\cos\theta_{10}\dot{p}+\omega_p^2 P_2^* A_6^*\sin\theta_{10} p\\ &-\omega_p P_3^* A_6^*\sin\theta_{10}\dot{p}+\omega_p^2 P_3^* A_6^*\cos\theta_{10} p\ ) \end{aligned} \tag{25}$$

$$D_{se}(p,\,h) = \frac{\rho B^2}{m_p}\frac{\rho B^2}{m_h}\Omega_{h,p}\,(\omega_p P_1^* H_5^* \cos\theta_{11}\dot{p} + \omega_p^2 P_1^* H_5^* \sin\theta_{11} p - \omega_p P_4^* H_5^* \sin\theta_{11}\dot{p} + \omega_p^2 P_4^* H_5^* \cos\theta_{11} p + \omega_p P_1^* H_6^* \cos\theta_{12}\dot{p} + \omega_p^2 P_1^* H_6^* \sin\theta_{12} p - \omega_p P_4^* H_6^* \sin\theta_{12}\dot{p} + \omega_p^2 P_4^* H_6^* \cos\theta_{12} p) \tag{26}$$

and the phase lags are

$$\theta_9 = \theta_{\alpha p} + 3\pi/2 \tag{27}$$

$$\theta_{10} = \theta_{\alpha p} \tag{28}$$

$$\theta_{11} = \theta_{hp} + 3\pi/2 \tag{29}$$

$$\theta_{12} = \theta_{hp} \tag{30}$$

$$\theta_{\alpha p} = arctg\frac{2\xi_\alpha \omega_\alpha \omega_p}{\omega_\alpha^2 - \omega_p^2} \quad (0^o < \theta_{\alpha p} < 90^o) \tag{31}$$

$$\theta_{hp} = arctg\frac{2\xi_h \omega_h \omega_p}{\omega_h^2 - \omega_p^2} \quad (\omega_h > \omega_F,\ 0^o < \theta_{hp} < 90^o,\ \omega_h > \omega_F,\ 90^o < \theta_{hp} < 180^o) \tag{32}$$

By solving these motion equations, the relationship between oscillation frequencies, damping ratios and the aerodynamic configuration of a bridge deck that defined by a set of flutter derivatives can be quantitatively established.

2.3. Description of coupling effects

In order to qualitatively clarify the coupling effects and quantitatively calculate the participation level of motion in each DOF both before and at the flutter onset, the flutter modality vectors defined in a three-dimensional coordinate system are introduced in the 2d-3DOF method. In this three-dimensional coordinate system, the x axis is for heaving DOF, the y axis is for swaying DOF and the z axis is for torsional DOF. The position of the endpoint for a flutter modality vector on the unit spherical surface reveals the relative paticipation level of each DOF before and at the flutter onset. For motions with the torsional frequency, the endpoint of the vector is

$$V_\alpha = \left(\frac{\rho B^2 \Omega_{h\alpha}\sqrt{H_2^{*2} + H_3^{*2}}}{m_h C_\alpha},\ \frac{\rho B^2 \Omega_{p\alpha}\sqrt{P_2^{*2} + P_3^{*2}}}{m_p C_\alpha},\ \frac{1}{C_\alpha}\right) \tag{33}$$

In which

$$C_\alpha = \sqrt{\left(\frac{\rho B^2}{m_h}\Omega_{h,\,\alpha}\sqrt{H_2^{*2} + H_3^{*2}}\right)^2 + \left(\frac{\rho B^2}{m_p}\Omega_{p,\,\alpha}\sqrt{P_2^{*2} + P_3^{*2}}\right)^2 + 1} \tag{34}$$

For motions with the heaving frequency, the endpoint of the modality vector is

$$V_h = \left(\frac{1}{C_h},\ \frac{\rho B^2 \Omega_{ph}\sqrt{P_1^{*2} + P_4^{*2}}}{m_p C_h},\ \frac{\rho B^4 \Omega_{\alpha h}\sqrt{A_1^{*2} + A_4^{*2}}}{I C_h}\right) \tag{35}$$

In which

$$C_h = \sqrt{1 + \left(\frac{\rho B^2}{m_p}\Omega_{ph}\sqrt{P_1^{*2} + P_4^{*2}}\right)^2 + \left(\frac{\rho B^4}{I}\Omega_{\alpha h}(A_1^{*2} + A_4^{*2})\right)^2} \tag{36}$$

For motions with the lateral frequency, the endpoint of the modality vector is

$$V_p = \left(\frac{\rho B^2 \Omega_{hp}\sqrt{H_5^{*2} + H_6^{*2}}}{m_h C_p}, \frac{1}{C_p}, \frac{\rho B^4 \Omega_{\alpha p}\sqrt{A_5^{*2} + A_6^{*2}}}{I C_p}\right) \tag{37}$$

In which

$$C_p = \sqrt{\left(\frac{\rho B^2}{m_h}\Omega_{hp}\sqrt{H_5^{*2} + H_6^{*2}}\right)^2 + 1 + \left(\frac{\rho B^4}{I}\Omega_{\alpha p}\sqrt{A_5^{*2} + A_6^{*2}}\right)^2} \tag{38}$$

If only two degrees of freedom are considered, i.e., heaving and torsion, the flutter modality vectors are defined in a two-dimensional coordinate system, in which the x axis is for heaving DOF and the y axis is for torsional DOF, and the endpoint of each flutter modality vector locates on a unit circle. Thus the expressions are also simplified.

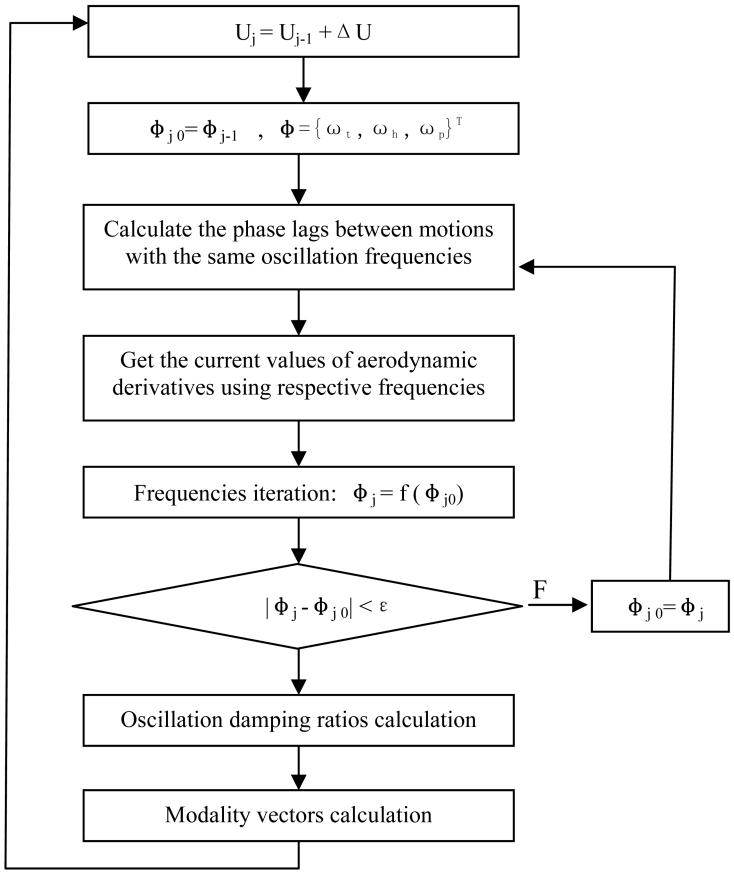

Fig. 1 2d-3DOF method flowchart

3. Two-dimensional three-degree-of-freedom coupling flutter analysis method

Based on above formulations, a two-dimensional three-degree-of-freedom coupling flutter analysis method (2d-3DOF method) that can simultaneously investigate the relationship between oscillation parameter of three degrees of freedom and aerodynamic derivatives obtained by wind tunnel testing with sectional model tests, and can clarify the coupling effect of each DOF in flutter instability is developed. The flowchart of this method is shown in Fig. 1 (Yang 2002).

By solving three motion equations, the aerodynamic stiffness and aerodynamic damping of a two-dimensional bridge section can be expressed by the combination of aerodynamic derivatives and phase lags between motions having the same oscillation frequency, and the participation level of motion in each DOF both before and at the flutter onset is described by corresponding flutter modality vectors (Yang 2002, Yang2003). Based on such information, the investigation on the flutter mechanism of long-span bridges and controlling mechanism for aerodynamic flutter control measures can be carried out.

4. Investigation on two typical bridge deck sections

Generally speaking, there are two typical bridge deck sections for long-span bridges which are shown in Fig. 2. Section A is a streamline box girder section which is popularly adopted in the construction of long-span suspension bridges and cable-stayed bridges, such as the Great Belt East Bridge, Jiangyin Yangtze Bridge, the 2nd Nanjing Yangtze Bridge etc. While Section B is a two-isolated-girder section which has been used in some long-span cable-stayed bridges with steel concrete composite decks, such as Nanpu Bridge, Yangpu Bridge etc. With the 2d-3DOF coupling flutter analysis method and sectional model wind tunnel tests, the flutter mechanism of these two typical bridge deck sections were investigated.

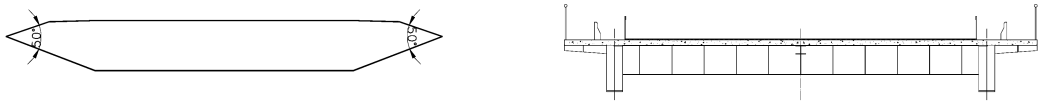

Section A Section B

Fig. 2 Typical bridge deck sections

4.1. Identification of aerodynamic derivatives

The aerodynamic derivatives of both sections were experimentally identified by a free vibration method in the TJ-1 boundary layer wind tunnel of the State Key Laboratory for Disaster Reduction in Civil Engineering of Tongji University with 1 : 70 sectional models. The testing results of aerodynamic derivatives versus reduced wind speeds of both sections are shown in Fig. 3 and Fig. 4 respectively.

These figures indicate that the major difference exists in the evolution trend of A_2^* with reduced wind speeds. While A_2^* of the streamline box section decreases continuously with the increase of reduced wind speed, A_2^* of the two-isolated-girder section turns from negative to positive at a relatively low reduced wind speed. The value evolution of A_1^*, H_2^* and H_3^* with reduced wind speeds are also different. These differences reflect the discrepancy in the aerodynamic

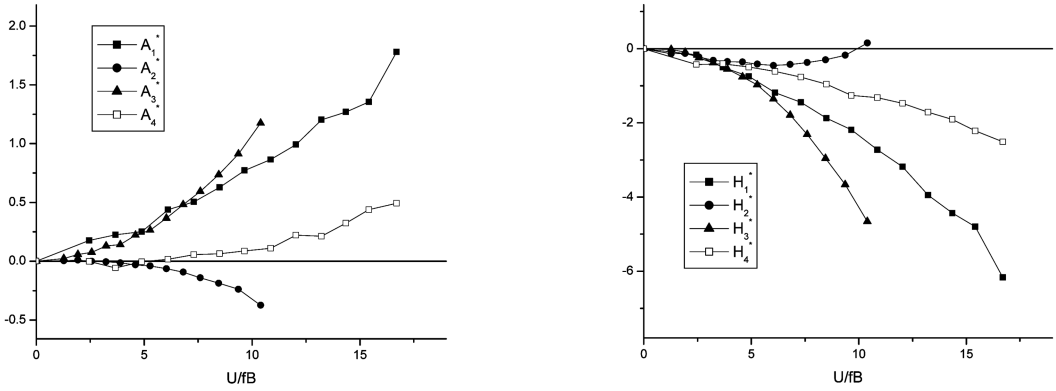

Fig. 3 Aerodynamic derivatives of section A

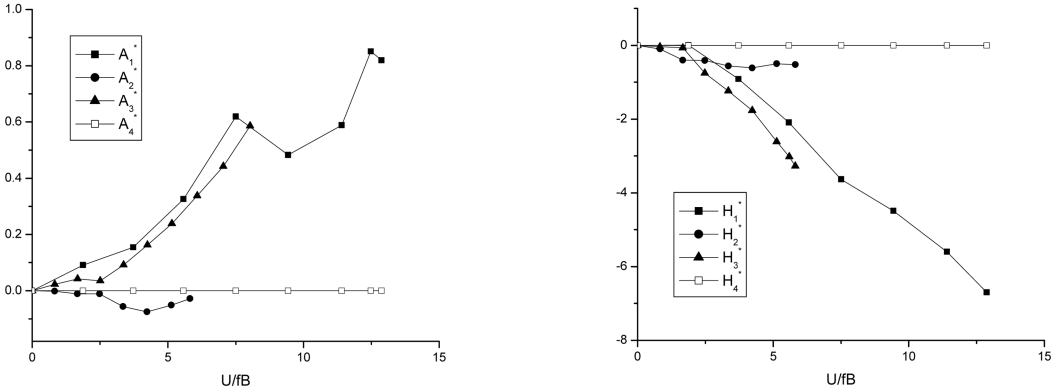

Fig. 4 Aerodynamic derivatives of section B

configurations of two typical bridge deck sections, thus affects the aerodynamic behavior of respective bridge deck.

4.2. Influence of aerodynamic damping

With those obtained aerodynamic derivatives, flutter analysis was carried out by the 2d-3DOF method. Calculation results show that it is the negative aerodynamic damping of motions with the torsional frequency that leads to the flutter onset of both sections. This is the common ground of the flutter-driving mechanism for the two typical bridge deck sections. However, as mentioned before, the self-excited pitching moment has three items due to the coupling effects of motions in different DOFs in the structure-wind interaction, so that the aerodynamic damping of motions with the torsional frequency not only comes from torsional motion directly, but also comes from coupled heaving and swaying motions indirectly. The detailed aerodynamic damping ratios are shown in Fig. 5. Because only torsional and heaving DOFs are included in the current study, the aerodynamic damping ratio in torsion can be represented by the summation of five parts as shown in Fig. 5.

It can be seen from Fig. 5 that the main difference between the flutter mechanism of the two typical bridge deck sections. Although the aerodynamic damping caused by the coupling effects

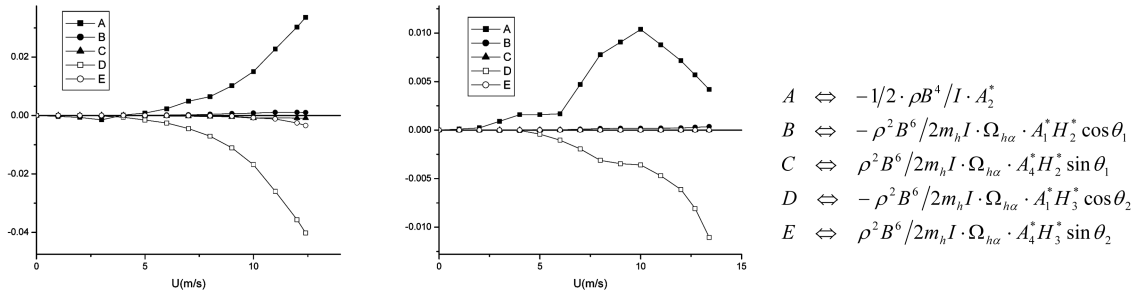

section A section B

Fig. 5 Aerodynamic damping ratio

between torsional and heaving motions especially Part D with the reference of $A_1{}^* H_3{}^*$ is the main driving power leading to the negative aerodynamic damping and also the flutter onset, the damping which is caused directly by torsional motion, i.e., Part A with the reference of A_2^*, is the stabilizing resource for section A even when wind speed reaching high, but for section B it drops down with the increase of wind speed and gradually lost the stabilizing contribution.

It is also shown in Fig. 5 that for typical sections like section B whose A_2^* turn from negative to positive at relatively low wind speed the main driving force leading to the flutter onset may not be the aerodynamic damping which is caused directly by torsional motion (Part A), the coupling effects between torsional and heaving motions still play a more important role. So judging the flutter performance of this type of bridge deck sections only by analyzing the curve of A_2^* is incorrect.

4.3. Contribution of aerodynamic stiffness

Fig. 6 shows the detailed five parts of aerodynamic stiffness of motions with the torsional frequency. For both sections the aerodynamic stiffness mainly comes from torsional motion directly. However, aerodynamic stiffness which comes from DOF coupling effects plays a more notable role for streamline box sections.

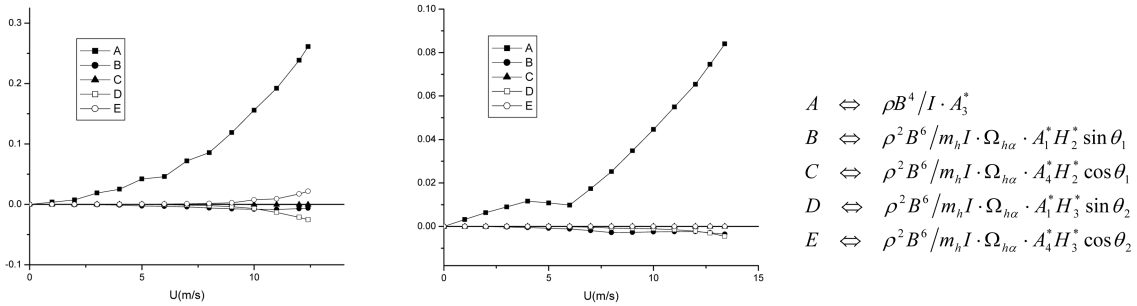

section A section B

Fig. 6 Aerodynamic stiffness

4.4. Participation levels of torsional and heaving DOFs

The participation level of each DOF at the flutter onset condition for each section was analyzed

through flutter modality vectors which are shown in Fig. 7. It can be seen that the difference in flutter mechanism of two typical bridge deck sections is also revealed in the position of modality vectors: for section A the participation level of heaving motion is higher than that of section B, which implies a more significant coupling effect in motions of different DOFs. Together with the flutter modality vectors of section A are shown the flutter modality vectors of ideal thin plate with the same structural dynamic properties. The participation level of heaving motion for thin plate is much higher, and the DOF coupling effect of this section is dramatic. The flutter modality vectors of a rectangular section which has a width-to-depth ratio of 3.5 with the same dynamic properties as section B are shown with the modality vectors of section B, and the participation level of heaving DOF is rather low.

In order to investigate the effect of variation of structural frequency ratio ε, which is defined as structural torsional frequency divided by bending frequency, on the participation level of each DOF, some alternative frequency ratios are chosen in the current study while the original frequency ratio is about 2.0 for both sections. The results are also shown in Fig. 7. It can be seen from the figures that with the decrease of structural frequency ratio the participation level of heaving motion in the torsional flutter gets higher for both sections, which implies a stronger coupling in the motions of different DOFs before and at the flutter onset.

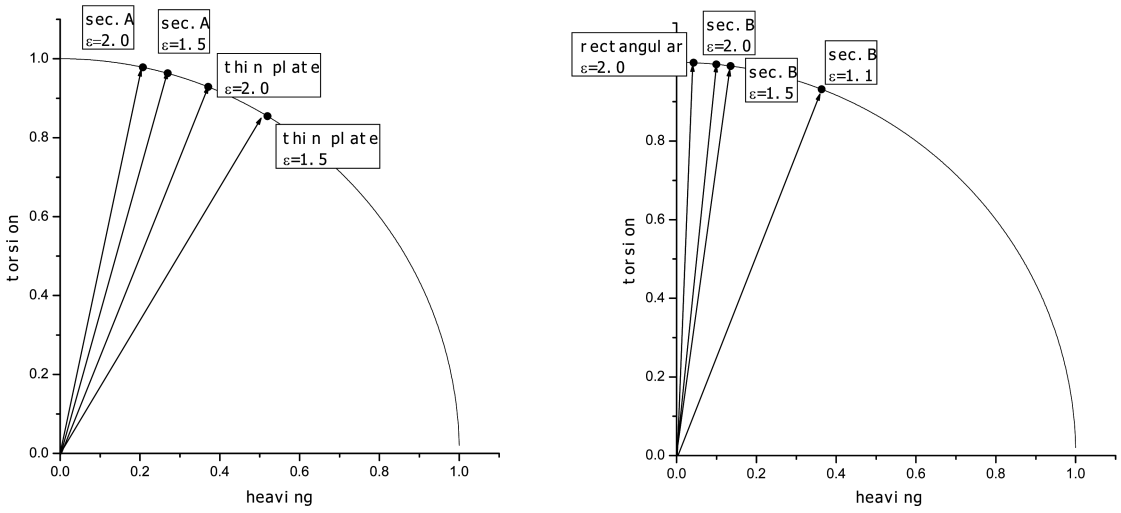

Fig. 7 Flutter modality vector

5. Investigation on central slotting

If a long-span bridge is predicted to have its intrinsic limit in the aspect of aerodynamic instability, it is necessary to adopt some countermeasures, for example, central stabilizer and central slotting, to improve flutter property to meet with the appropriate wind resistance requirements. Theoretical and experimental investigations reported in the literature (Walshe 1997, Richardson 1981, Fung 1993) support the conclusion that the application of central slotting in the box section can improve aerodynamic stability of suspension bridges. The feasibility study of Gibraltar Bridge shows that not only there is a clear trend for the slotted-box section to become increasingly aeroelastically stable for increasing deck vent width but also this increase ratio of critical wind

speeds with vent width can be fitted to the Power-law expressions by means of the least squares method (Larsen 1998). The invited presentation "On Aerodynamic Limit to Suspension Bridges" on the 11th International Conference on Wind Engineering demonstrated that an enough-widely slotted box deck can provide a 5,000 m span-length suspension bridge with high enough critical wind speed over 80m/s (Xiang 2003). It should be noted that, however, although the engineering feasibility of slotted box girders has been studied to some extent, there is no real project of suspension bridge with employing slotted box girders for the purpose of aerodynamic stability improvement.

Based on a real engineering project, Xihoumen Bridge in China, the flutter controlling effect and mechanism of central slotting were investigated. In order to establish the experimental evidence linking vent width to aerodynamic stability, the ratio of vent width b to the solid box width B was respectively set to b/B=0, 0.2, 0.4, 0.6, 0.8, and 1.0 in wind tunnel tests with simplified cross sections described in Fig. 8.

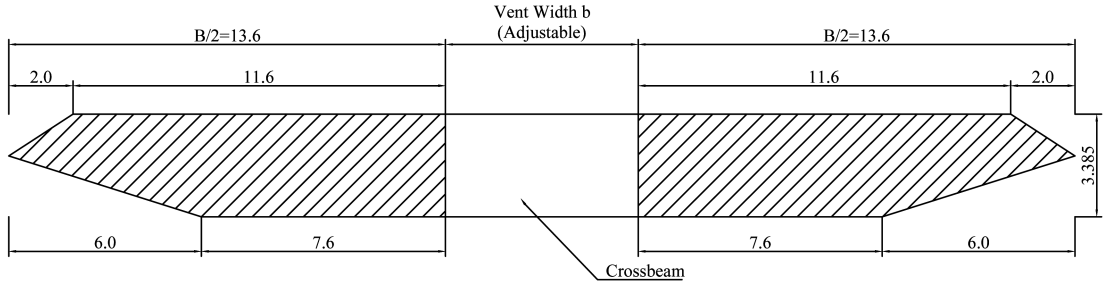

Fig. 8 Simplified cross section (Unit: m)

5.1. Critical wind speeds

The wind tunnel testing of the slotted box girders was carried out in smooth flow at Tongji University's TJ-1 Boundary Layer Wind Tunnel with the working section of the 1.8 m width, the 1.8 m height and the 15m length. The flutter critical speeds of sections with different vent widths and under different wind angles of attack are tested, and eight flutter derivatives of these cross sections are identified for theoretical investigations of stabilizing mechanism.

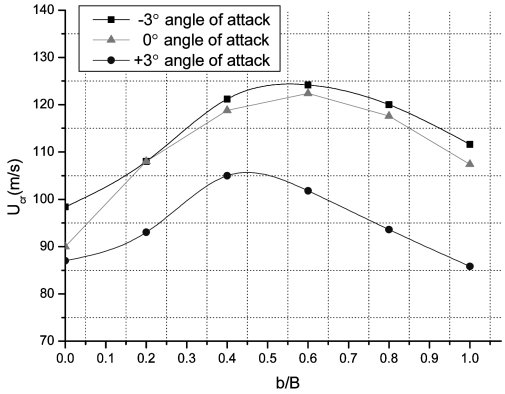

Fig. 9 Measured critical wind speed

Table 1 Measured wind speed (m/s)

b/B	+3°	0°	-3°	Min
0	87.0	90.0	98.4	87.0
0.2	93.0	108.0	108.0	93.0
0.4	105.0	118.8	121.2	105.0
0.6	101.8	122.4	124.2	101.8
0.8	93.6	117.6	120.0	93.6
1.0	85.8	107.4	111.6	85.8

The most important wind tunnel test result links the critical wind speed of the slotted box cross section to the vent width for the cases at the attack angles of +3°, 0° and -3° is summarized in Fig. 9 and Table 1.

It can be seen from Fig. 9 or Table 1 that the stabilizing effectiveness of slotted box girders generally depends upon two important characteristics including width of central vent and angle of attack. Fig. 9 demonstrates a clear fact that the values of critical wind speeds vary with angle of attack for all cases with various widths of central vent. In particular, the critical wind speed increases with the relative width of central vent from b/B = 0 to b/B = 0.4 at the +3° angle of attack, and from b/B = 0 to b/B = 0.6 at the attack angle of 0° and -3°, respectively, but decreases with the relative width from b/B = 0.4 to b/B = 1.0 at +3° and from b/B = 0.6 to b/B = 1.0 at 0° and -3°, respectively.

Since aerodynamic instability takes place whenever a bridge is exposed to wind speeds above the critical value at the attack angle covering from +3° to -3°, the dominant factor of aerodynamic stability is the minimum value among three critical wind speeds corresponding to the attack angle of +3°, 0° and -3°. It is interesting to see that all minimum values for certain vent width are at the +3° angle of attack.

In order to quantitatively evaluate stabilizing effect of central vent, the relative factor of critical wind speed is defined as follows:

$$\eta = \frac{U_{crb}}{U_{cro}} \tag{39}$$

where U_{cro} is the critical wind speed without central vent; and U_{crb} is the critical wind speed with the vent width of b. The relation between relative factor η and relative vent width b/B is represented in Fig. 10 for the +3° angle of attack. The minimum value of the relative factor η, which was calculated at the +3° angle of attack, is always greater than unit for all relative vent width b/B = 0 to b/B = 0.8, and reach the maximum value of 1.21 at b/B = 0.48 following the fitted curve of the measured critical wind speeds.

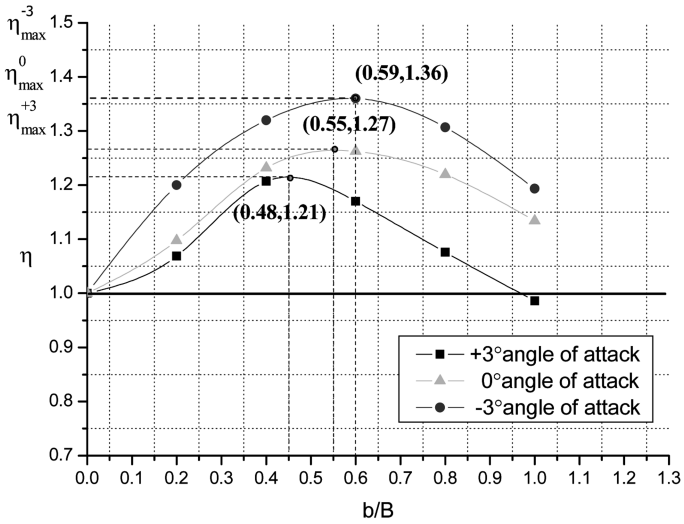

Fig. 10 Relative factor of critical wind speed

5.2. Aerodynamic damping

As mentioned before, the aerodynamic damping ratio in torsion can be represented by the summation of five parts due to coupling effects between torsional and heaving motions. Fig. 11 describes the evolution of the five parts of the aerodynamic damping ratio in torsion for the slotted cross section with b/B = 0, b/B = 0.2 and b/B = 0.4 at the +3° angle of attack. For all three cases, Part A with the reference of A_2^* is always positive and makes the greatest contribution to aerodynamic stability among five parts for all three cases, while Part D with the reference of $A_1^* H_3^*$ keeps negative all the way and causes the worst influence of aerodynamic stability. The influence of Part E is helpful to stability but with the smaller effect, and Both Parts B and C have smallest value. The characteristics of aerodynamic damping for cross section with b/B = 0 is just like that of Section A in the previous study due to similarity in aerodynamic configuration. After central slot is applied, for cross section with b/B = 0.2, the value of positive aerodynamic damping Part A gets a little larger, while the evolution of Part D is like being controlled to some extent and the absolute value gets smaller. When the vent width increases to b/B = 0.4, these controlling effects become more evident as the value of Part A gets even larger and the absolute value of Part D gets even smaller. Therefore, the oscillation system becomes more aerodynamically stable. The total damping ratios including structural one and these five parts are shown in Fig. 12 for six cases with the relative vent widths from b/B = 0 to b/B = 1.0 at the +3° angle of attack.

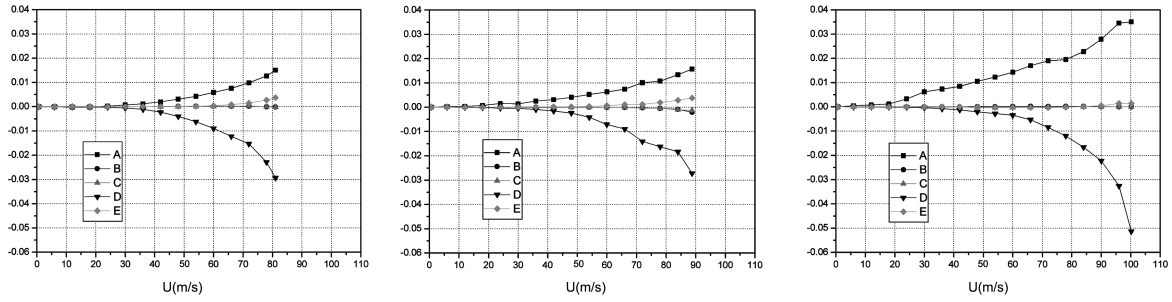

a) b/B = 0 b) b/B = 0.2 c) b/B = 0.4

Fig. 11 Aerodynamic damping ratios

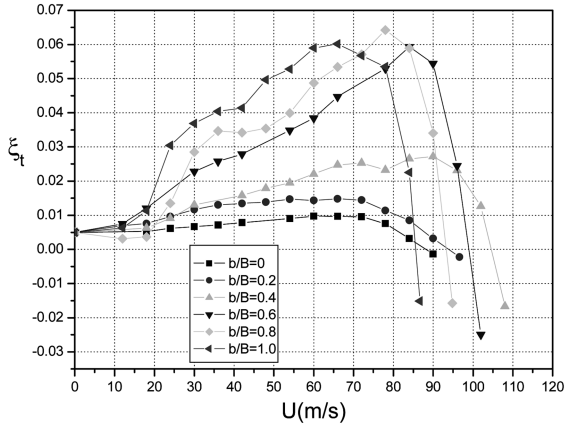

Fig. 12 Total damping ratios

Table 2 DOF participation level

b/B	U_{cr}(m/s)	α	h
0	87.0	0.967	0.254
0.2	93.0	0.949	0.315
0.4	105.0	0.938	0.348
0.6	101.8	0.940	0.341
0.8	93.6	0.942	0.335
1.0	85.8	0.968	0.249

5.3. DOF participation level

For the above-mentioned six cases in two-degree vibration, the DOF participation level and the corresponding critical wind speed at the flutter onset can be represented in Table 2. The box section with the relative vent width of $b/B = 0.4$ at the $+3^{o}$ angle of attack has the highest level of heaving DOF participation and the greatest critical wind speed, while the box section with the relative width of $b/B = 1.0$ and without vent have almost the same lowest values of both coupling effect of heaving DOF participation and critical wind speed. In general, it can be concluded that the more heaving DOF participate at the flutter onset, the higher critical wind speed can be reached.

5.4. Further discussion

The present results in Fig. 10 deserve a different trend of critical wind speeds versus vent width from previous aerodynamic studies on suspension bridges with slotted box girders, for example, the stability results reported by Larsen, *et al*. (1998) and Sato, *et al*. (2001). Both the Larsen's and Sato's results demonstrate the same trend that critical wind speed monotonously increases with the increase of vent width, while the present result show a new way that the evolution curve have two different regions, the increasing region from b/B=0 to b/B=0.4 and the decreasing one from b/B=0.4 to b/B=1.0.

A plausible explanation of this difference is that aerodynamic stability of a slotted section is very sensitive to the sharp angle of triangular outboard edges, and thus must be carefully predicted with individual section. Another likely explanation is that aerodynamic force is quite different acting on a slotted section with outboard edges of a symmetric triangular and an asymmetric triangular, and must lead to the flutter onset with different generated mechanism. The combination of these two effects is speculated to govern the evolution trend of critical wind speed through vent width. It is supposed by the authors that there might be three kinds of possible evolution trends with the variation of the shape (symmetric or asymmetric) and the value of edge angles, that is, mono increase such as the models used by Larsen and Sato, mono decrease for example square outboard edges mentioned in the literature(Yang 2002, Sato 2001), and the new one from increase to decrease based on the present study. Of course, this supposition needs further studies to be proven with particular shape and value of edge angles in the future.

6. Conclusions

A two-dimensional three-degree-of-freedom flutter analysis method (2d-3DOF method) was developed to simultaneously investigate the relationship between oscillation parameters and aerodynamic derivatives of three degrees of freedom, and to clarify the coupling effects of degrees of freedom in flutter instability. With this method, the flutter mechanism of two typical bridge deck sections, box girder section and two-isolated-girder section, was numerically investigated through comparisons of aerodynamic damping, aerodynamic stiffness and participation levels of torsional and heaving DOFs. Both differences and common ground in these two typical flutter phenomena are summarized. Based on the recent project of Xihoumen Bridge in China, aerodynamic stabilization and its mechanism of central slotting for long-span bridges were carefully investigated through experimental investigation and theoretical analysis. Some new findings in the evolution trend of critical wind speed through central vent width are finally explained.

Acknowledgements

The work described in this paper is part of a research project financially supported by the National Science Foundation of China (Grant 50608059). Sincere appreciation should also go to Zou X.J. of Tongji University for her contributions to the related wind tunnel tests and analyses work.

References

Como, M., Ferraro, S. D. and Grimaldi, A. (2005), "A parametric analysis of the flutter instability for long span suspension bridges", *Wind Struct.*, **8**(1), 1-12.

Ding, Q.S., Chen, A.R. and Xiang, H.F. (2002), "A state space method for coupled flutter analysis of long-span bridges", *Struct. Eng. Mech.*, **14**(4), 491-504

Fung, Y.C. (1993), *An Introduction to the Theory of Aeroelasticity*, Dover Publications, New York.

Ge, Y.J. *et al*. (2003), *Study of Aerodynamic Performance and Vibration Control of Xihoumen Bridge* (in Chinese), Technical Report of the State Key Laboratory for Disaster Reduction in Civil Engineering, No. WT200320.

Hua, X. G., Chen, Z. Q., Ni, Y. Q. and Ko, J. M. (2007), "Flutter analysis of long-span bridges using ANSYS", *Wind Struct.*, **10**(1), 61-82

Larsen, A. (1993), "Aerodynamic aspects of the final design of the 1624m suspension bridge across the Great Belt", *J. Wind Eng. Ind. Aerodyn*., **48**, 261-285.

Larsen, A. and Astiz, M.A. (1998), "Aeroelastic consideration for the Gibraltar Bridge feasibility study", *Bridge Aerodynamics*, Larsen & Esdahl (eds), Balkema, Rotterdam, 165-173.

Matsumoto, M., Kobayashi, Y., Niihara, Y., Shirato, H. and Hamasaki, H. (1995), "Flutter mechanism and its stabilization of bluff bodies", *Proceedings of the 9th International Conference on Wind Engineering*, New Delhi, 827-837.

Matsumoto, M. (2000), "Flutter classification of bridge girders", *Proceedings of the 1st International Symposium on Wind and Structures for the 21st Century*, Cheju, Korea, 39-79.

Richardson, J.R. (1981), *The Development of the Concept of the Twin Suspension Bridge*, National Maritime Institute, NMIR125.

Sato, H., Toriumi, R. and Kusakabe, T. (2001), "Aerodynamic characteristics of slotted box girders", *Bridges into the 21st Century*, 721-728.

Selberg, A. (1963), "Aerodynamic effect on suspension bridges", *Proceedings of International Symposium on Wind Effects on Buildings and Structures*, Teddington, England, **2**, 462-486.

Simiu, E. and Scanlan, R.H. (1996), *Wind Effects on Structures (3rd Edition)*, John Wiley & Sons, New York.

Walshe, D.E., Twidle, G.G. and Brown, W.C. (1997), "Static and dynamic measurements on a model of a slender bridge with perforated deck", *International Conference on the Behaviour of Slender Structures*, The City University, London, England.

Xiang, H.F. and Zhang, R.X. (1999), "On mechanism of flutter and unified flutter theory of bridges", In Larsen, Larose & Livesey (eds), *Wind engineering into 21st century*, Rotterdam, Balkema.

Xiang, H.F. *et al*. (2003), *Wind Resistance Study on Runyang Suspension Bridge across Yangtze River*, Technical Report of the State Key Laboratory for Disaster Reduction in Civil Engineering, No. WT200005.

Xiang, H.F. and Ge, Y.J. (2003), "On aerodynamic limit to suspension bridges", *Proceedings of the 11th International Conference on Wind Engineering*, Texas, USA, 65-80.

Yang, Y.X. (2002), *Two-Dimensional Flutter Mechanism and its Applications for Long-Span Bridges* (in Chinese), Ph.D Thesis Supervised by H.F. Xiang, and Y.J. Ge, Tongji University, China.

Yang, Y.X., Ge, Y.J. and Xiang, H.F. (2002), "Coupling effects of degrees of freedom in flutter instability of long-span bridges", *Proceedings of the 2nd International Symposium on Advances in Wind and Structures*, Busan, Korea, 625-632.

Yang, Y.X., Ge, Y.J. and Xiang, H.F. (2003), "3DOF coupling flutter analysis for long-span bridges", *Proceedings of the 11th International Conference on Wind Engineering*, Texas, USA, 925-932.

CC